Thieme

Impact of Patient Alignment on Image Quality in C-Arm Computed Tomography – Evaluation Using an ACR Phantom

Einfluss der Patientenausrichtung auf die Bildqualität in der C-Bogen-Computertomografie – Evaluation mithilfe eines ACR-Phantoms

Authors
Babak Alikhani[1], Julius Renne[2], Sabine Maschke[2], Jan B. Hinrichs[2], Frank K. Wacker[2], Thomas Werncke[2]

Affiliations
1 Center for Radiology and Nuclear Medicine, DIAKOVERE Hospital gGmbH, Hannover, Germany
2 Institute for Diagnostic and Interventional Radiology, Hannover Medical School, Hannover, Germany

Key words
C-arm flat-panel detector computed tomography, flat-panel detector, patient alignment, heel effect, image quality

received 13.09.2019
accepted 03.08.2020

Bibliography
DOI https://doi.org/10.1055/a-1238-2802
Published online: 2020
Fortschr Röntgenstr

ISSN 1438-9029

Correspondence
Dr. Babak Alikhani
Center for Radiology and Nuclear Medicine,
DIAKOVERE Hospital gGmbH, Hannover, Germany
Tel.: ++ 49/5 11/2 89 24 35
babak.alikhani@diakovere.de

ZUSAMMENFASSUNG

Ziel Der Einfluss der Patientenausrichtung und des Heel-Effekts auf die Bildqualität einer C-Bogen-Flachbilddetektor-Durchleuchtungseinheit (CACT) wurde untersucht.

Material und Methoden Ein ACR-Phantom wurde in entgegengesetzten Richtungen entlang der z-Achse auf dem Patiententisch platziert (Setup A und B). Die Messungen wurden an einem CACT mit neuartigen Flachdetektoren durchgeführt. Die Bilddaten wurden mit 3 verschiedenen Untersuchungsprotokollen und 4 Faltungskernen rekonstruiert. Die Hochkontrastauflösung mithilfe der Modulationsübertragungsfunktion (MTF) und die Niederkontrastsauflösung unter Verwendung des Bildrauschens, des Signal-Rausch-Verhältnisses (SNR) und des Kontrast-Rausch-Verhältnisses (CNR) wurden bestimmt. Außerdem wurden die Dosisintensitätsprofile „frei in Luft“ gemessen.

Ergebnisse MTF in Setup B ist höher als in Setup A ($p < 0{,}01$). Das Rauschen in Setup A für die Luft- und Knocheneinsätze war höher als in Set-up B ($p > 0{,}05$). Ein umgekehrter Verlauf wurde für die Einsätze aus Polyethylen, Wasseräquivalent und Acryl beobachtet. SNR für alle Einsätze ist umgekehrt proportional zum Bildrauschen. Ein systematisch ansteigender oder abnehmender Trend von CNR konnte nicht beobachtet werden ($p > 0{,}05$). Das vom Detektorsystem gemessene Intensitätsprofil „frei in Luft“ zeigte, dass der Heel-Effekt senkrecht zur z-Achse und nicht parallel dazu verläuft.

Schlussfolgerung Die Patientenausrichtung hat einen geringen Einfluss auf die Bildqualität von CACT. Dieser Effekt beruht nicht auf dem Hell-Effekt, sondern durch die asymmetrische Rotation des CACT-Arms.

Kernaussagen:

- Der Einfluss der Patientenausrichtung und des Heel-Effektes auf die Bildqualität von CACT wurde analysiert.
- Die Patientenausrichtung hat einen geringen Einfluss auf die physikalischen Bildqualitätsparameter wie Rauschen, SNR und MTF.
- Dieser Effekt beruht hauptsächlich auf der asymmetrischen Rotation des CACT-Arms.

ABSTRACT

Purpose To evaluate the influence of patient alignment and thereby heel effect on the image quality (IQ) of C-arm flat-panel detector computed tomography (CACT).

Materials and Methods An ACR phantom placed in opposite directions along the z-axis (setup A and B) on the patient support was imaged using CACT. Image acquisition was performed with three different image acquisition protocols. The images were reconstructed with four convolution kernels. IQ was assessed in terms of high contrast using the modulation transfer function (MTF) and low contrast by assessing the image noise, signal-to-noise ratio (SNR) and contrast-to-noise ratios (CNR) as well as the reliability of density measurements. Furthermore, the dose intensity profiles were measured free-in-air.

Results The MTF in setup B is higher than the MTF measured in setup A ($p < 0.01$). The image noises measured in setup A for the air and bone inserts were higher compared to those measured in setup B ($p > 0.05$). Opposite behavior has been

observed for the polyethylene, water-equivalent and acrylic inserts. The SNR for all inserts is inversely related to the image noise. A systematically increasing or decreasing trend of CNR could not be observed ($p > 0.05$). The intensity profile measured by the detector system free-in-air showed that the anode heel effect is perpendicular to the z-axis.

Conclusion The patient alignment has a minor influence on the IQ of CACT. This effect is not based on the X-ray anode heel effect but is caused mainly by the non-symmetrical rotation of CACT.

Key Points:

- The impact of patient alignment and thereby the heel effect on the image quality of CACT was analyzed.
- The patient alignment has a minor influence on the physical parameters related to image quality, such as noise, SNR, and MTF.
- This effect is based mainly on the non-symmetrical rotation of CACT.

Citation Format

- Alikhani B, Renne J, Maschke S et al. Impact of Patient Alignment on Image Quality in C-Arm Computed Tomography – Evaluation Using an ACR Phantom. Fortschr Röntgenstr 2020; DOI 10.1055/a-1238-2802

Introduction

C-arm flat-panel detector computed tomography (CACT) allows acquisition and reconstruction of CT-like images in a flat-panel angiography system providing cross-sectional information during an interventional procedure. In addition to the diagnostic value, CACT images can be fused with real-time fluoroscopy, thus considerably expanding the diagnostic and therapeutic options of an angiographic system [1]. Therefore, the use of CACT is on the rise in many radiologic and neuroradiologic interventions [2, 3]. Although the low-contrast performance of CACT is inferior compared to multi-detector CT (MDCT) systems, comparative studies using the same radiation exposure for both techniques confirm higher spatial resolution for CACT compared to MDCT [4, 5]. Furthermore, it has been shown that quantitative measurements in the same region are sufficiently reliable [6]. However, due to the conical beam geometry used in CACT as well as in cone-beam CT (CBCT) with wide aperture angles, it is to be expected that the homogeneity of the radiation field and thus the image quality of CACT and CBCT is significantly influenced by the heel effect of the X-ray tube anode.

Compared to MDCT, the maximum X-ray tube power of CACT is lower. Furthermore, the flat-panel detector installed in CACT reaches its maximum quantum efficiency at an X-ray high voltage of around 80 to 90 kVp [7, 8]. Therefore, the pre-filtration of CACT is normally restricted to the inherent X-ray tube filtration of 2.5 mmAl and the use of bow-tie filters which can increase image quality is omitted. The lower beam hardening of CACT compared to conventional CT combined with the use of lower tube potential results in a softer X-ray spectrum of CACT. These technical limitations particularly favor beam hardening and photon starvation artifacts [9].

If the angular distribution of an X-ray tube spectrum or the heel effect is aligned along the patient table in CACT, the image quality might be affected by the patient alignment and could have an impact on the reliability of quantitative measurements. Previous investigations demonstrated the artifacts, for example, intensity inhomogeneities or errors induced in quantitative densitometry, caused by the heel effect and its influence on the image quality in CBCT [11, 12].

To the best of our knowledge, the impact of patient alignment on CACT image quality has never been studied.

The purpose of this study was to investigate the impact of patient alignment on the image quality represented by physical image parameters.

Materials and Methods

Phantom

In order to assess image quality in terms of high and low contrast resolution in this study, an ACR phantom (American College of Radiology CT accreditation phantom, Model 464, Gammex-RMI, Middleton, Wisconsin) was used in this study. This phantom consists of a water-equivalent material and contains four modules [13]. Each module has a diameter of 20 cm with a length of 4 cm. A sketch and an AP projection of an ACR phantom are shown in ▶ **Fig. 1a, b**. The modules are designed to determine image quality parameters, such as CT number and low- and high-contrast resolution. Since the influence of patient alignment can be greatest at the end of the phantom, only the first and the last modules of the phantom were utilized in this study. These modules are described as follows:

Using the first module, module 1, the spatial resolution or high contrast can be determined. This module has eight aluminum bar resolution patterns, i. e., 4, 5, 6, 7, 8, 9, 10, and 12 lp/cm, which are illustrated in ▶ **Fig. 1c**. The depth of the patterns is 3.8 cm along the z-axis.

The CT numbers of different materials can be determined using module 4, which contains five cylinders of materials with different densities. The materials and their densities are as follows: air (0 g/cm^3), bone (1.95 g/cm^3), polyethylene (0.94 g/cm^3), water-equivalent cylinder (1 g/cm^3), and acrylic (1.18 g/cm^3).

Each cylinder has a diameter of 25 mm and a length of 4 cm, except for the water-equivalent cylinder with a diameter of 50 mm. ▶ **Fig. 1d** shows a CT image of module 4. The experimental setups A and B are shown in ▶ **Fig. 2a, b**, respectively.

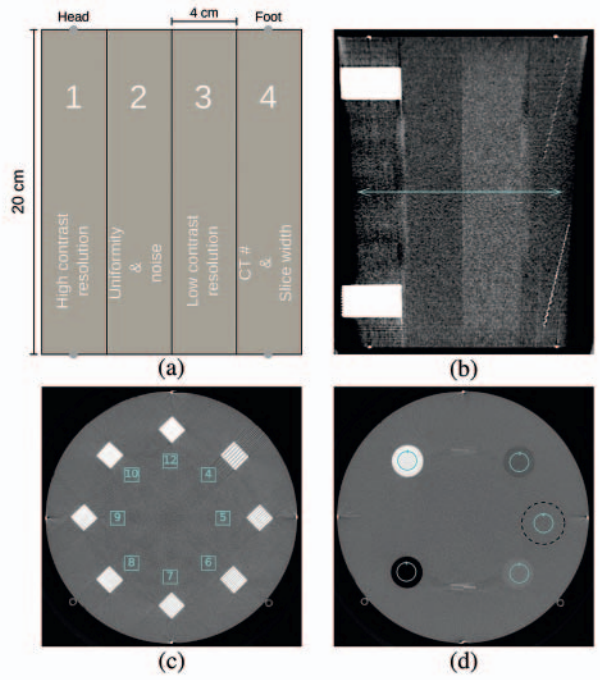

▶ **Fig. 1** **a** Sketch of an ACR phantom. **b** ACR phantom imaged by CACT. The solid (blue) arrow indicates the range of selected images for noise determination along the z-axis (see the Results section). **c** Module 1: The numbers in square present the count of line pairs per cm (lp/cm). **d** Module 4: The numbers indicate different materials: ① Air, ② Bone, ③ Polyethylene, ④ Water-equivalent material, ⑤ Acrylic. The black, dashed ring indicates the water-equivalent cylinder.

▶ **Abb. 1** (**a**) Skizze eines ACR-Phantoms. (**b**) CACT-Aufnahme eines ACR-Phantoms. Zur Bestimmung des Rauschens entlang der z-Achse wurde der mit dem blauen Pfeil markierte Bereich ausgewählt. (**c**) Modul 1. Die Zahlen präsentieren die Anzahl der Linienpaare pro cm (lp/cm). (**d**) Modul 4. Die Zahlen geben verschiedene Materialien an: ① Luft, ② Knochen, ③ Polyethylen, ④ Wasseräquivalentes Material, ⑤ Acryl. Der schwarze, gestrichelte Kreis zeigt den Wasser-äquivalenten Zylinder.

Image acquisition

The phantom was placed in 2 positions (setups A, B) on the patient table in the isocenter of the CACT – as follows:

For setup A the phantom was placed with the high-contrast segment (module 1) feet first. For setup B the phantom was placed head first.

CACT of the phantom was acquired using a monoplane, ceiling-mounted, angiographic system (Artis Q; Siemens Healthineers, Forchheim, Germany) using a CACT preset (6S DynaCT-Body, Dyna CT; Siemens Healthineers, Forchheim, Germany) with a 6 s rotation run from −100° to 100° without additional filtering. Along this 200° rotation, 397 projections with a constant detector dose were acquired. The chosen acquisition geometry was a table-side trajectory with a C-arm rotation around the phantom that usually performed for body scans.

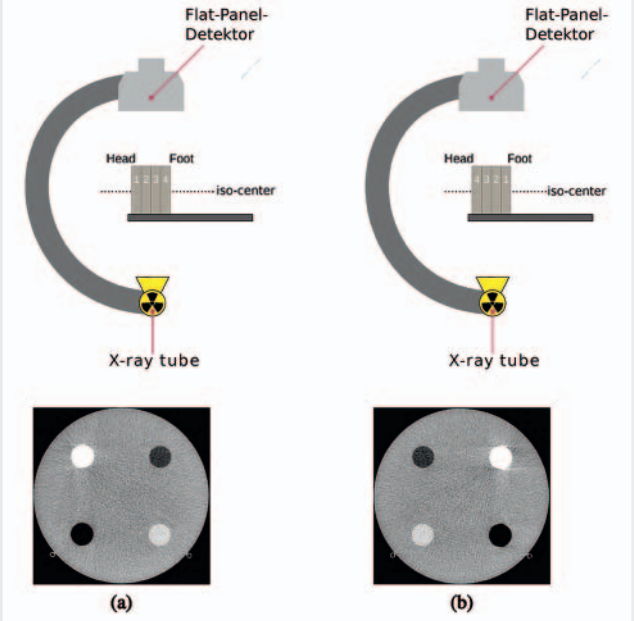

▶ **Fig. 2** **a** Setup A. **b** Setup B. An image of module 4 depicts the different orientations of the phantom on the patient support.

▶ **Abb. 2** (**a**) Setup A. (**b**) Setup B. Ein Bild des Moduls 4 illustriert die unterschiedliche Ausrichtung des Phantoms auf dem Patiententisch.

CACT was equipped with a 3-foci Gigalix X-ray tube (Siemens Healthineers, Forchheim Germany) and a 30 × 40 cm flat-panel detector system [14]. The source-to-detector distance was 119.8 cm. The phantom was placed at the isocenter of the system.

The measurements were performed using three different image acquisition protocols with X-ray tube voltages of 81, 102, and 125 kVp using the large focal spot (0.7 mm). ▶ **Table 1** presents the image acquisition protocols of the measurements.

Images were reconstructed with four different convolution kernels: normal, hard, soft, and very soft with a reconstructed slice thickness of 0.49 mm.

Afterwards, the images were exported and analyzed using plug-ins and macros for the software program ImageJ (open-source image analysis software, version 1.50d; https://www.imagej.nih.gov/ij/).

The 2D intensity profile of the X-ray tube was measured using 55 kVp irradiating the detector free-in-air. 1D profiles were calculated by averaging the 2D profile along two axes parallel and perpendicular to the patient support using 200 lines. The 1D profile can be utilized to calculate the anode angle α of the X-ray tube. The analytical model for heel effect described by Dixon et al. [15, 16] was used. The heel effect function ρ(x) can be approximated with an accuracy of better than 0.16 % as

$$p(x) \approx 1 - \beta(E, \bar{\mu}) \cdot \frac{x}{F \cdot \tan\alpha}\left(1 + \frac{x}{F \cdot \tan\alpha}\right) \quad (1)$$

where β represents the anode attenuation along the central ray of the X-ray beam. Furthermore, β is a function of the weighted aver-

▶ **Table 1** Image acquisition protocols of the measurements.

▶ **Tab. 1** Akquisitionsparameter der Messungen.

X-ray tube voltage (kVp)	setup	X-ray tube current (mA)	dose area product (cGy*cm²)
81	A	253	1879.6
81	B	255	1892.0
102	A	91	1226.6
102	B	92	1232.7
125	A	39	1039.5
125	B	39	1045.1

age of attenuation coefficients $\bar{\mu}$ over the X-ray spectrum (E) with a value of 0.28 at 120 kVp being determined empirically. F denotes the distance of the focal spot to the detector. For the calculation of the anode angle only, the slope is considered.

Image Quality Assessment

The high-contrast resolution of imaging systems was measured in terms of MTF using the bar patterns in module 1 of the phantom. Droege and Morin [17] devised a practical method for the MTF determination. This method was based on the standard deviation measurements of the pixel values within an image of bar patterns. Therefore, 10 × 10 mm² square-shaped regions of interest (ROIs) were placed within bar patterns and the background.

An image set including 50 images was utilized for the MTF calculation. Using the CT numbers in the ROIs and their standard deviations, MTF values for each spatial frequency (lp/cm) were calculated.

A Gaussian fit was used to estimate the 50 %, 10 %, and 2 % MTF values for all reconstruction kernels.

Furthermore, for quantifying the effect of the phantom alignment on the CT numbers, the CT numbers of the inserts in both setups were determined.

The low contrast resolution was assessed using the image noise, signal-to-noise ratio (SNR), and contrast-to-noise ratio (CNR).

The image noise is defined as the standard deviation of the voxel density. The noise parallel to the patient support (z-axis) was determined using ROIs with an area of about 300 mm² at the center of images along the ACR phantom. The noise profile by selection of 250 slices for different X-ray tube peak voltages was calculated in the central part of the phantom. To avoid the impact of cone-beam artifacts on the results, images at the border regions of the phantom were deselected (see ▶ **Fig. 1**, top right). Furthermore, using the uniform module (module 2), the image noise perpendicular to the patient support (x-axis) was also calculated. Mean averages using 25 images were calculated.

SNR is defined as the ratio between the mean CT number and its standard deviation, i. e.,

$$SNR = \frac{\overline{CT}\#}{\alpha} \quad (2)$$

CNR is defined as

$$CNR = \frac{\overline{CT}\#_{insert} - \overline{CT}\#_{bg}}{\alpha_{bg}} \quad (3)$$

where $\overline{CT}\#_{insert}$ is the mean CT number within a defined ROI. $\overline{CT}\#_{bg}$ and σ_{bg} denote the CT numbers of the background and the corresponding standard deviation in an ROI with the same area.

Image noise, SNR, and CNR were assessed using the density inserts placed in module 4 of the ACR phantom. ROIs of about 250 mm² were placed in the density inserts, in order to measure the absorption of each insert. The corresponding standard deviations were calculated in ROIs with the same area placed at the middle of module 4. Mean averages were calculated using 25 images.

The normal kernel was utilized to calculate noise, SNR, and CNR, while MTF was determined using four kernels.

For the evaluation of statistical significance, paired two-sided t-tests were applied. A p-value of < 0.05 was considered statistically significant.

Results

▶ **Fig. 3** shows the intensity profiles of CACT. On the top of this figure, the 2D profile is depicted, while the bottom plots present the profiles along (z-axis) and perpendicular (x-axis) to the patient support, respectively. The intensity profile on the z-axis is an average of 200 rows and shows an intensity variation of about 4 %. The slope of the 1D profile along the x-axis by averaging 200 rows caused by the heel effect to deliver an anode-angle of $\alpha = (8.84 \pm 0.02)$ degrees. The real anode angle obtained from the technical manual of the facility with a 3-foci Gigalix X-ray tube is 11.5 degrees. The main difference between the measured value and real value of the anode angle is the neglecting of the focus size ("point source") in the equation (1) [15].

The difference is also based on the energy dependency of the factor β. The measurement with another X-ray tube high voltage, e. g. 120 kVp, might deliver a different anode angle. Furthermore, the measurement of the 2D intensity profile was performed with the grid, which has an impact on the determined anode angle from the measurement.

MTF values determined for both setups are shown in ▶ **Fig. 4**. For both setups the MTF assessed using a sharp convolution kernel shows the highest high-contrast resolution, while the MTF calculated by a very soft kernel denotes the lowest high-contrast resolution. Furthermore, 50 %, 10 %, and 2 % MTF values for all reconstruction kernels are listed in ▶ **Table 2**.

The differences in MTF values measured by setups A and B for all convolution kernels and at all used X-ray tube voltages are statistically significant ($p < 0.01$).

The related CT numbers of inserts with different densities for all X-ray tube voltages measured by setups A and B were calculated and presented in ▶ **Table 3**. As expected, the measured CT numbers behaved linearly relative to material density. Due to the beam-hardening effect of the photon fluence spectra, the CT numbers decrease with X-ray tube voltage and material density.

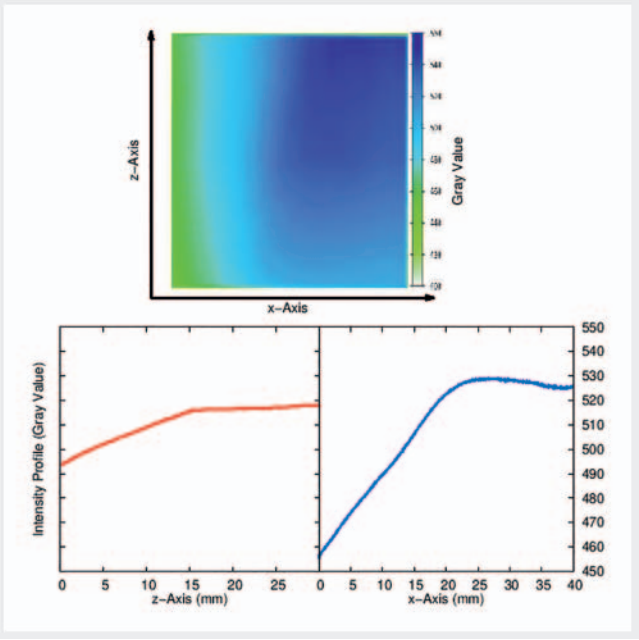

▶ **Fig. 3** 2D intensity profile of the detector (top). 1D profile along the patient support (bottom, left) and perpendicular to the patient support (bottom, right). The profile along the x-axis indicates that the heel effect is perpendicular to the patient support. Using equation (1) and 1D profile along the x-axis, an anode angle of $\alpha = (8.84 \pm 0.02)$ degrees was determined. We presume that the kink in the profile along the z-axis is caused by the use of a grid between the X-ray tube anode and the patient support.

▶ **Abb. 3** 2D-Intensitätsprofil (oben). 1-D-Profil entlang des Patiententischs (unten, links) und senkrecht zum Patiententisch (unten, rechts). Das Profil entlang der x-Achse zeigt an, dass der Heel-Effekt senkrecht zum Patiententisch ist. Unter Verwendung von Gleichung (1) und 1-D-Profil entlang der x-Achse lässt sich ein Anodenwinkel von $\alpha = (8{,}84 \pm 0{,}02)$ Grad bestimmt. Der Knick im Profil entlang der z-Achse wird vermutlich durch die Verwendung eines Gitters zwischen der Röntgenröhre und dem Patiententisch verursacht.

Based on this effect, the largest difference in the CT numbers at the X-ray tube voltages of 81, 102, and 125 kVp for bone insert was observed.

Except the polyethylene insert at the X-ray tube voltage of 81 kVp and the acrylic insert at the X-ray tube voltages of 81 and 102 kVp, the difference between the CT numbers measured by setup A and setup B at all X-ray tube voltages for the inserts was considered statistically significant.

The image noise within the same ROIs for all materials is presented in ▶ **Fig. 5**. The image noise measured in setup A for the air and bone inserts was systematically higher compared to that measured in setup B, on average about 3 % and 4 % for the air and bone inserts ($p > 0.05$), respectively.

The opposite behavior has been observed for the polyethylene, water-equivalent, and acrylic inserts. The corresponding image noises were on average about 4 %, 6 %, and 2 % lower in setup A compared to those measured in setup B. ▶ **Fig. 6** shows the SNR values ($p > 0.05$).

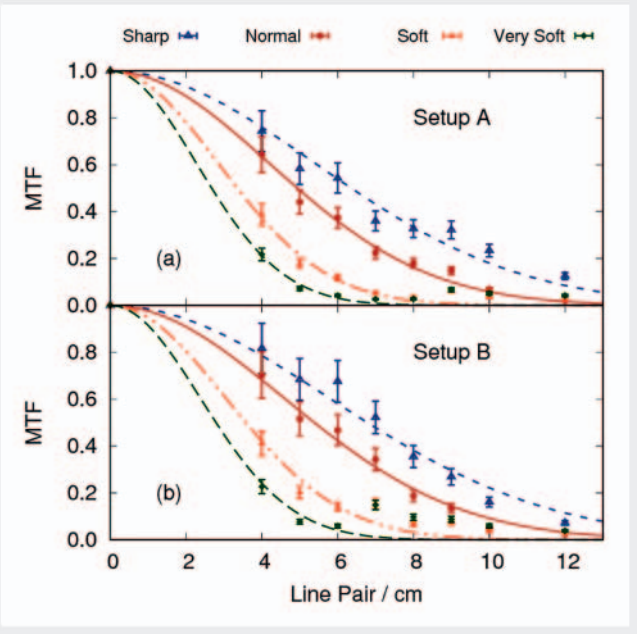

▶ **Fig. 4** MTF calculated for different convolution kernels for an X-ray tube voltage of 102 kVp. The fit model is the Gaussian function. **a** Setup A. **b** Setup B.

▶ **Abb. 4** Berechnete MTF und Gauß-Fitfunktionen für verschiedene Faltungskerne bei einer Röhrenspannung von 102 kVp. (**a**) Setup A. (**b**) Setup B.

As expected, the SNR for all inserts behaves inversely to the image noise. This can be explained by equation (2) and the almost constant CT numbers of the inserts measured in setups A and B, which are already presented in ▶ **Table 3**.

The CNR values for five inserts are shown in ▶ **Fig. 7**. Except for the water-equivalent insert, the CNR values for all inserts calculated in setup A are on average about 4 % higher than those calculated in setup B ($p > 0.05$). CNR for water-equivalent insert is small with corresponding large uncertainties.

The noise profiles parallel and perpendicular to the patient supports for both setups are presented in ▶ **Fig. 8**. The staircase-shaped behavior of the noise plot measured along the z-axis is because of the different attenuation properties of the phantom modules. The radiation intensity in the case of the uniform module has been less attenuated than in the case of other modules, which is reflected by the gap in the noise diagram (▶ **Fig. 8** (left)). The image noise that increases at the middle of images along the x-axis is based on the cupping effect.

Discussion

The presented investigation demonstrated a minor impact of patient alignment on CACT image quality.

The 2D profile measurement showed that the change in image quality parameters, such as MTF, SNR, and CNR, along the patient support (z-axis) was not based on the heel effect of the X-ray tube anode. The intensity profile of CACT measured by the detector

▶ **Table 2** 50 %, 10 %, and 2 % MTF for all reconstructions.

▶ **Tab. 2** 50 %, 10 %, und 2 % MTF für alle Rekonstruktionen.

convolution Kernels	50 % MTF			10 % MTF			2 % MTF		
	setup A	setup B	p-value	setup A	setup B	p-value	setup A	setup B	p-value
normal	4.9 ± 0.1	5.4 ± 0.1	< 0.001	9.0 ± 0.2	9.8 ± 0.2	< 0.001	11.7 ± 0.2	12. 8 ± 0.2	< 0.001
sharp	6.4 ± 0.2	6.8 ± 0.2	< 0.001	11.6 ± 0.3	12.4 ± 0.3	< 0.001	15.1 ± 0.4	16.1 ± 0.4	< 0.001
soft	3.4 ± 0.1	3.6 ± 0.1	< 0.001	6.1 ± 0.1	6.5 ± 0.2	< 0.001	8.0 ± 0.2	8.5 ± 0.3	< 0.001
very soft	2.7 ± 0.1	2.8 ± 0.2	0.002	4.9 ± 0.2	5.1 ± 0.4	0.002	6.4 ± 0.3	6.6 ± 0.5	0.009

▶ **Table 3** CT numbers of different materials measured by setup A (a) and setup B (b).

▶ **Tab. 3** CT-Zahlen für verschiedene Materialien in Setup A und Setup B.

inserts	81 kVp			102 kVp			125 kVp		
	setup A	setup B	p-value	setup A	setup B	p-value	setup A	setup B	p-value
air	−870 ± 4	−880 ± 4	< 0.001	−882 ± 5	−893 ± 5	< 0.001	−900 ± 5	−914 ± 5	< 0.001
polyethylene	−110 ± 4	−109 ± 4	0.38	−134 ± 5	−127 ± 5	< 0.001	−192 ± 5	−181 ± 5	< 0.001
water-equivalent	10 ± 5	4 ± 5	< 0.001	−37 ± 5	−32 ± 5	< 0.001	−112 ± 5	−99 ± 6	< 0.001
acrylic	88 ± 6	85 ± 5	0.06	57 ± 6	58 ± 6	0.56	−12 ± 6	−5 ± 6	< 0.001
bone	1127 ± 7	1163 ± 6	< 0.001	930 ± 7	948 ± 6	< 0.001	724 ± 7	743 ± 6	< 0.001

system free-in-air showed an intensity gradient perpendicular to the patient support (x-axis). This finding indicates that the anode heel effect is not in the longitudinal direction to the z-axis.

Due to small varying of the radiation dose, given by dose area product, ranging from 0.5 % to 0.7 % for all X-ray tube voltages, the difference in image quality parameters, such as image noise, SNR, CNR, and MTF, measured by both setups cannot be attributed to the radiation dose.

The observed differences in image quality, dependent on the phantom alignment, are mainly caused by the incomplete rotation of CACT around the z-axis. This incomplete rotation leads to inhomogeneous irradiation of the object as compared to conventional CT. This inhomogeneous dose distribution in the object/phantom results in asymmetrical beam hardening and scattering [10, 18] which lead to the orientation-dependent image quality observed in this study. This assertion was clearly noted by the measured image noises for the bone (+ 4 %) and acrylic (−2 %) inserts as the noise values showed reversed variation for setups A and B. The same but inverse effect could be observed for the air (+ 3 %) and polyethylene (−6 %) inserts. In addition, we verified the influence of the incomplete rotation of CACT on image quality by rotating the phantom 180 degrees about its central axis, see ▶ **Fig. 9**. The noise values in the bone and polyethylene inserts in the left setup (▶ **Fig. 9a**) were lower than those measured in the right setup (▶ **Fig. 9b**) about 13 %. The inverse behavior has been observed for the air and acrylic inserts in the both setups (−12 %). While the SNR was increased for the air and acrylic inserts in the right setup, those values for the bone and polyethylene inserts were decreased. This is an indicator of the impact of phantom alignment on image quality.

Furthermore, the MTF was calculated using the method of Droege and Morin, which is based on the standard deviation (noise) measurements of the pixel values within the bar pattern. In both setups the high contrast inserts are irradiated differently. This also caused different noise values in both setups that leads to variation of the MTF.

The image noise increase at the middle along the x-axis is attributed to the cupping effect [19–21]. We assume that the difference in the image quality parameters is also based on the local dose that reaches the end of the phantom in both directions. Since the dose measurement using the ACR phantom was not possible, we focused our analysis on the noise determination along the z-axis, which reflects the local radiation dose. Both the intensity and noise profile along the z-axis validated the different doses along the patient support. The noise profile along the z-axis shows a reverse trend for both setups.

Up to now, the low- and high-contrast performance of CACT compared to MDCTs has been shown in previous studies. However, there is no study, to our knowledge, demonstrating a relationship between patient alignment and CACT image quality.

Bai et al. [22] assessed the image quality of a CACT system (Axiom Artis dTA; Siemens Healthcare, Forchheim, Germany) to

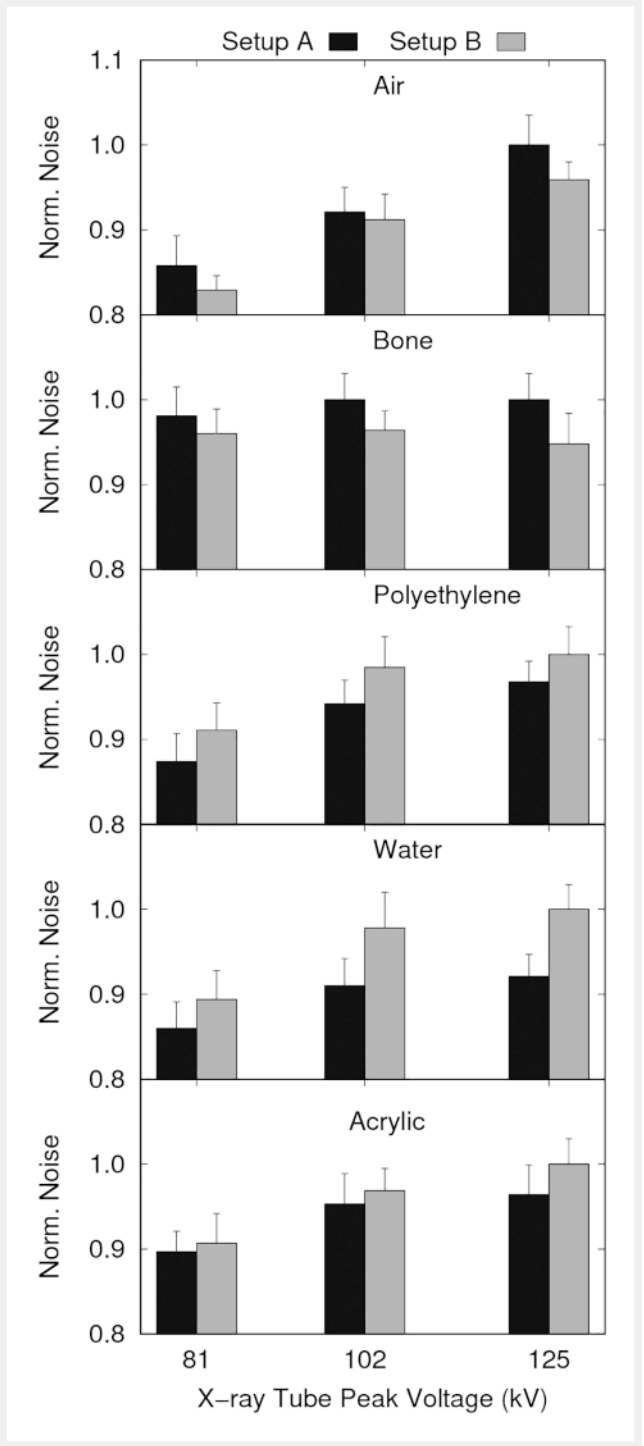

▶ **Fig. 5** Noise calculated in five inserts. Data are normalized to the maximum value of noise.

▶ **Abb. 5** Auf den Maximalwert normiertes Rauschen.

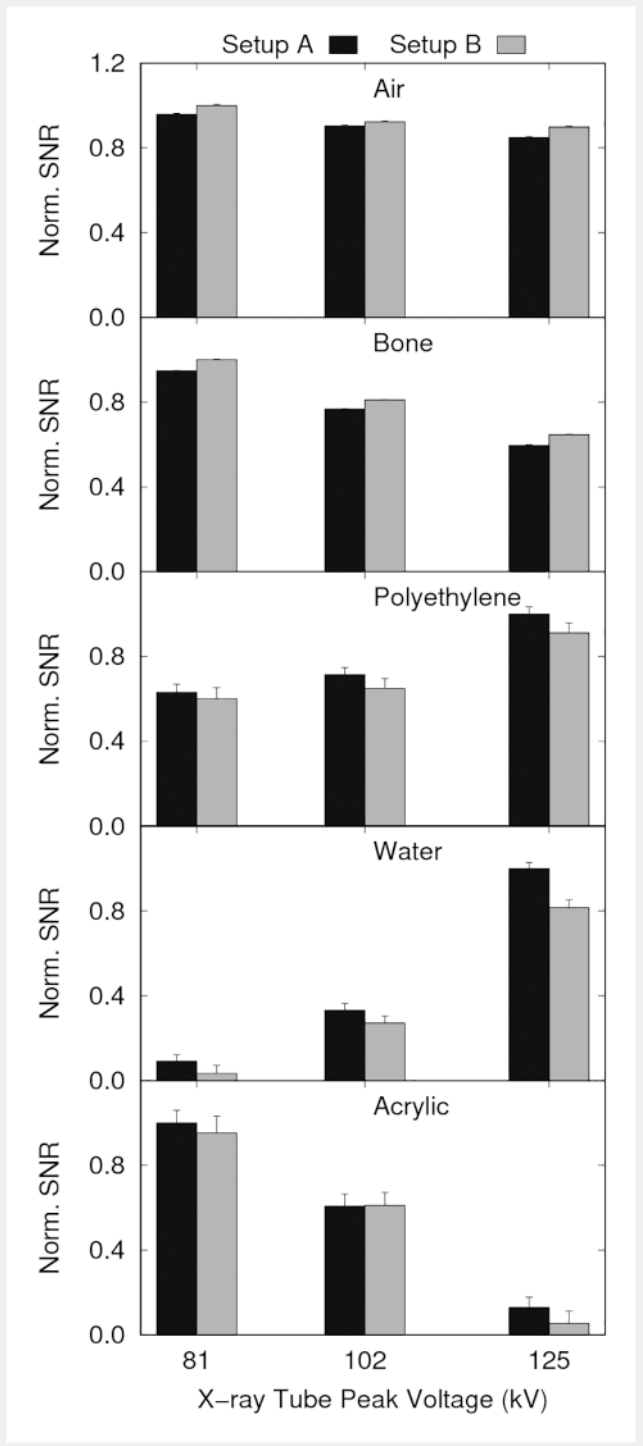

▶ **Fig. 6** SNR calculated in five inserts. Data are normalized to the maximum value of SNR.

▶ **Abb. 6** Auf den Maximalwert normiertes SNR.

that of two MDCT units (Lightspeed VCT; GE, Milwaukee, USA and Sensation Cardiac 64; Siemens Healthcare, Erlangen, Germany). A male Anderson Radiation Therapy 200 phantom was used and the radiation dose was measured with embedded thermoluminescence dosimeters (TLDs). The result indicated that CACT applied fewer doses to the phantom at a similar spatial resolution and low contrast detectability to both MSCT units. In another phantom and cadaveric study, Werncke et al. [5] compared the effective radiation dose and image quality between a CACT unit (Artis Zee Q; Siemens, Forchheim, Germany) with a standard 16-slice

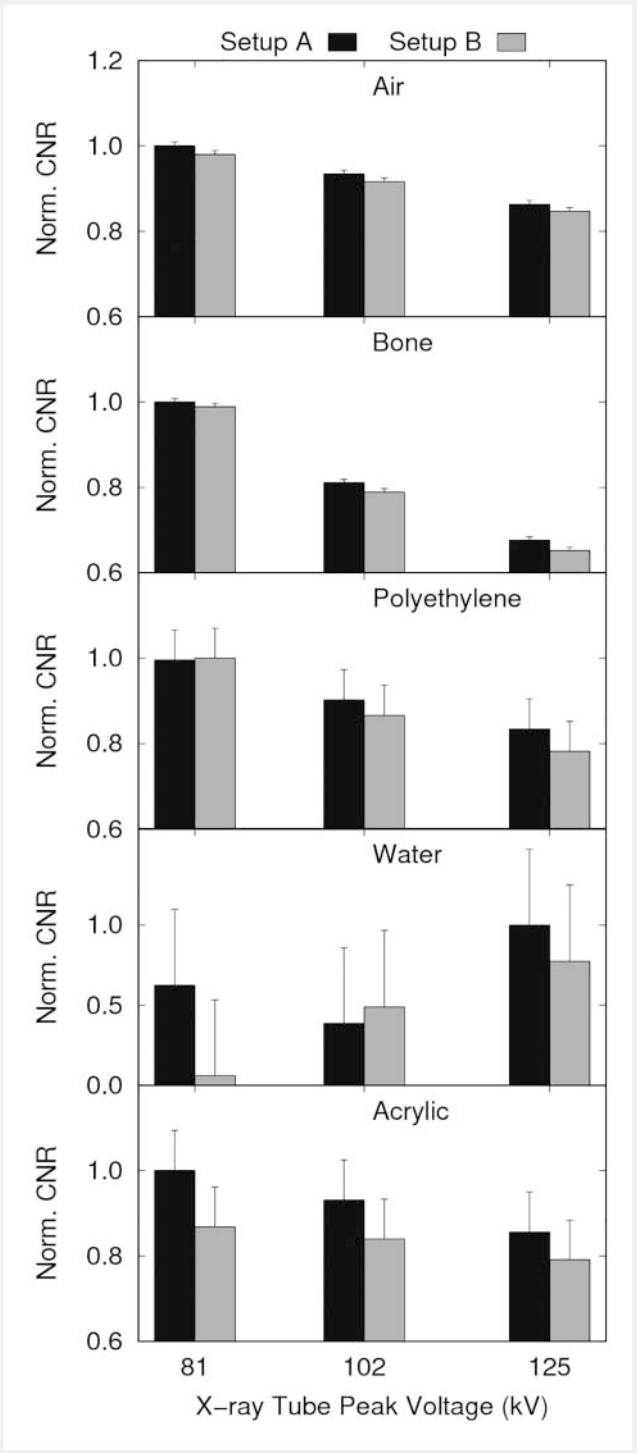

▶ **Fig. 7** CNR calculated in five inserts. Data are normalized to the maximum value of CNR.

▶ **Abb. 7** Auf den Maximalwert normiertes CNR.

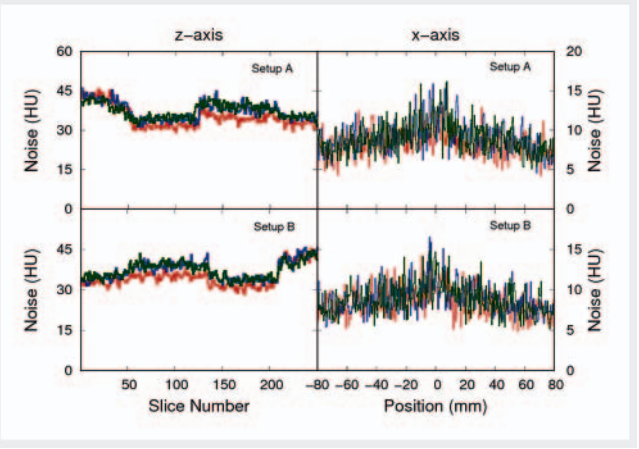

▶ **Fig. 8** Noise profile along the z-axis (left) and x-axis (right). The noise determination was performed by the setup A (top) and setup B (bottom). The red, blue, and green lines indicate the noise values for the X-ray tube peak voltages of 81, 102, and 125 kVp, respectively. The image noise increasing at the middle of images along the x-axis is based on the cupping effect.

▶ **Abb. 8** Profil des Rauschens entlang der z-Achse (links) und der x-Achse (rechts) in Setup A (oben) und Setup B (unten). Die roten, blauen und grünen Linien zeigen das Rauschen für die Röhrenspannungen von 81, 102 und 125 kVp. Die Erhöhung des Rauschens in der Mitte der x-Achse ist auf den Cupping-Effekt zurückzuführen.

MDCT unit (GE Lightspeed 16; GE Healthcare, Waukesha, Wisconsin). The radiation dose was determined using 100 TLDs placed in an anthropomorphic whole-body phantom (adult male phantom with arms, model 701 and model 701-10, CIRSinc, Norfolk, USA). The result of this study also showed an improvement in the spatial resolution with CACT compared to MDCT at the same radiation dose. However, recent studies indicate that, for the low range of the X-ray tube high voltage, the related low- and high-contrast image quality of CACT is similar to that of conventional CT [23, 24].

Our study has a number of limitations: First, we used a cylinder-shaped phantom with a radius of 20 cm which is only an approximation for a patient head. However, the advantage of this simplifying approach is that well-known artifacts, which are current limitations of C-arm CT, such as truncation artifacts and beam hardening, are avoided. The impact of truncation artifacts might be reduced by using recently presented software-based techniques, 3D camera systems [2], or extended-volume C-arm CT [3].

A more realistic phantom, for example with a spine, would introduce further artifacts depending on the orientation of the phantom and was therefore not used in this study.

The results of this study can be used for investigations of the head. Second, for obtaining the 2D and subsequent 1D intensity profiles and subsequently for calculating the anode angle, we irradiated the detector system, which has an energy dependency. Using another X-ray tube voltage, the anode angle would differ from 8.8 degrees. However, the main limitation is that the angular radiation dose distribution was missing. In order to obtain this information, a dose measurement using TLDs placed on the surface of the phantom had to be performed. This is time-consuming and would in our opinion not alter the obtained results.

Furthermore, it has to be mentioned that the standard C-arm calibration is conducted using a copper filter. Therefore, the heel effect is considered. Furthermore, due to the alignment of the

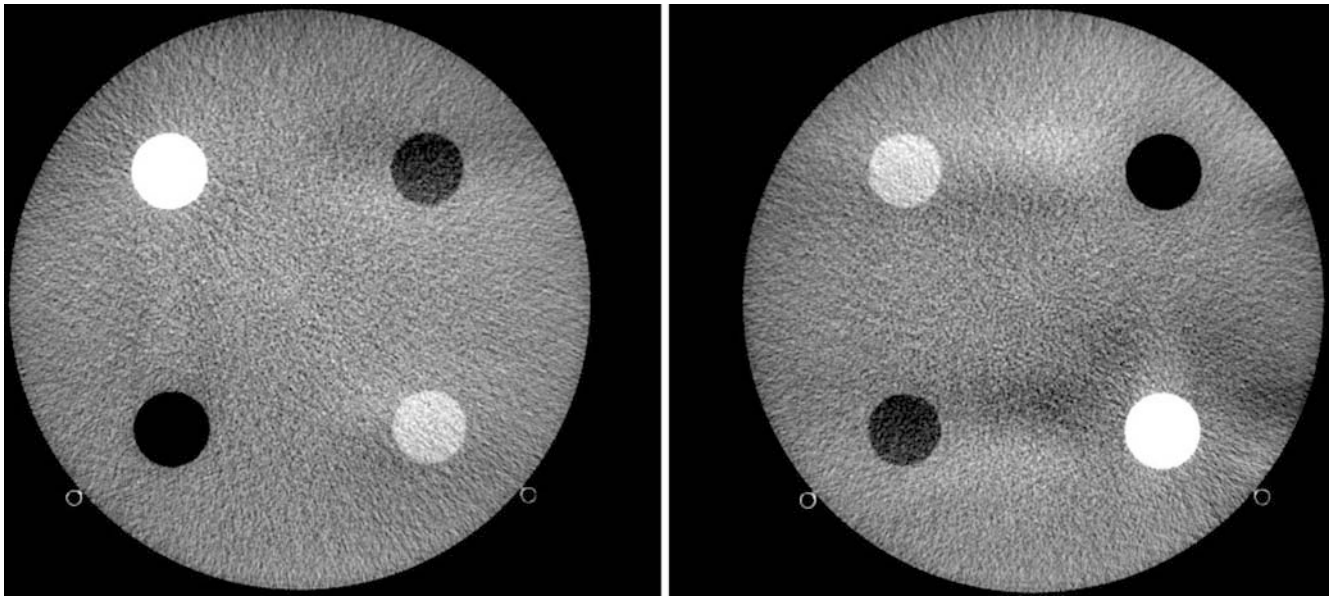

▶ **Fig. 9** Rotating the phantom 180 degrees about its central axis to verify the influence of incomplete rotation of the CACT on image quality.

▶ **Abb. 9** Um den Einfluss der unvollständigen Drehung des CACT auf die Bildqualität zu überprüfen, wurde das Phantom um 180 Grad um seine Mittelachse gedreht.

X-ray tube, any possible effect should be low as demonstrated in this study.

In conclusion, patient alignment has a minor influence on CACT image quality. This effect is caused mainly by the incomplete rotation of CACT.

Conflict of Interest

The authors declare that they have no conflict of interest.

References

[1] Smyth M, Sutton D, Houston J. Evaluation of the quality of CT-like images obtained using a commercial flat panel detector system. Biomed Imaging Interv J 2006; 2: e48

[2] Dörfler A, Struffert T, Engelhorn T et al. Rotational flat-panel computed tomography in diagnostic and interventional neuroradiology. Fortschr Röntgenstr 2008; 180: 891–898

[3] Braun H, Kyriakou Y, Kachelrieß M et al. The influence of the heel effect in cone-beam computed tomography: artifacts in standard and novel geometries and their correction. Phys Med Biol 2010; 55: 6005–6021

[4] Ott S, Struffert T, Saake M et al. Influence of different reconstruction parameters in the visualization of intracranial stents using c-arm flat panel CT angiography: experience in an animal model. Acta Radiol 2015; 57: 233–240

[5] Werncke T, Sonnow L, Meyer BC et al. Ultra-high resolution C-Arm CT arthrography of the wrist: Radiationdose and image quality compared to conventional multidetectorcomputed tomography. Euro J Radiol 2017; 89: 191–199

[6] Jones AK, Mahvash A. Evaluation of the potential utility of flat panel CT for quantifying relative contrast enhancement. Med Phys 2012; 39: 4149–4154

[7] Orth RC, Wallace MJ, Kuo MD. C-arm Cone-beam CT: General Principles and Technical Considerations for Use in Interventional Radiology. Journal of Vascular and Interventional Radiology 2008; 19: 814–820

[8] Fahrig R, Dixon R, Payne T et al. Dose and image quality for a cone-beam C-arm CT system. Med Phys 2006; 33: 4541–4550

[9] Rana N, Rawat D, Parmar M et al. Evaluation of external beam hardening filters on image quality of computed tomography and single photon emission computed tomography. Journal of Medical Physics 2015; 40: 198–206

[10] Zhang G, Marshall N, Jacobs R et al. Bowtie filtration for dedicated cone beam CT of the head and neck: a simulation study. Br J Radiol 2013; 86: 20130002

[11] Mori S, Endo M, Nishizawa K et al. Prototype heel effect compensation filter for cone-beam CT. Phys Med Biol 2005; 50: N359–N370

[12] Kusano Y, Uesaka S, Yajima K et al. Positional dependence of the CT number with use of a cone-beam CT scanner for an electron density phantom in particle beam therapy. Radiol Phys Tech 2013; 6: 241–247

[13] McCollough CH, Bruesewitz MR, McNitt-Gray MF et al. The phantom portion of the American college of radiology (ACR) Computed Tomography (CT) accreditation program: Practical tips, artifact examples, and pitfalls to avoid. Med Phys 2004; 31: 2423–2442

[14] Hinrichs JB, von Falck C, Hoeper MM et al. Pulmonary Artery Imaging in Patients with Chronic Thromboembolic Pulmonary Hypertension: Comparison of Cone-Beam CT and 64-Row Multidetector CT. J Vasc Inter Radiol 2016; 27: 361–368

[15] Dixon RL, Munley MT, Bayram E. An improved analytical model for CT dose simulation with a new look at the theory of CT dose. Med Phys 2005; 32: 3712–3728

[16] Dixon RL, Boone JM. Analytical equations for CT dose profiles derived using a scatter kernel of Monte Carlo parentage with broad applicability to CT dosimetry problems. Med Phys 2011; 38: 4251–4264

[17] Droege RT, Morin RL. A practical method to measure the MTF of CT scanners. Med Phys 1982; 9: 758–760

[18] Grimmer R, Kachelrieß M. Empirical binary tomography calibration (EBTC) for the precorrection of beam hardening and scatter for flat panel CT. Med Phys 2011; 38: 2233–2240

[19] Hunter AK, McDavid WD. Characterization and correction of cupping effect artifacts in cone beam CT. Dentomaxillofacial Radiol 2012; 41: 217–223

[20] Nagarajappa AK, Dwivedi N, Tiwari R. Artifacts: The downturn of CBCT image. J Inter Soc of Prev Comm Dentis 2015; 5: 440–445

[21] Barrett JF, Keat N. Artifacts in CT: Recognition and Avoidance. Radio-Graphics 2004; 24: 1679–1691

[22] Bai M, Liu B, Mu H et al. The comparison of radiation dose between C-arm flat-detector CT (DynaCT) and multi-slice CT (MSCT): A phantom study. Euro J Radiol 2012; 81: 3577–3580

[23] Schegerer AA, Lechel U, Ritter M et al. Dose and image quality of cone-beam computed tomography as compared with conventional multislice computed tomography in abdominal imaging. Invest Radiol 2014; 49: 675–684

[24] Jones AK, Odisio BC. Comparison of radiation dose and image quality between flat panel computed tomography and multidetector computed tomography in a hybrid CT-angiography suite. Journal of Applied Clinical Medical Physics 2020; 21: 121–127